Chin. Geogra. Sci. 2015 Vol. 25 No. 2 pp. 213–223
doi: 10.1007/s11769-014-0693-2

Springer Science Press
www.springerlink.com/content/1002-0063

Monitoring Soil Salt Content Using HJ-1A Hyperspectral Data: A Case Study of Coastal Areas in Rudong County, Eastern China

LI Jianguo[1], PU Lijie[1, 2], ZHU Ming[1], DAI Xiaoqing[1], XU Yan[1], CHEN Xinjian[1], ZHANG Lifang[3], ZHANG Runsen[1]

(1. *School of Geographic and Oceanographic Sciences*, *Nanjing University*, *Nanjing* 210023, *China*; 2. *Key Laboratory of the Coastal Zone Exploitation and Protection*, *Ministry of Land and Resources*, *Nanjing* 210023, *China*; 3. *School of Public Administration*, *Nanjing University of Finance & Economics*, *Nanjing* 210046, *China*)

Abstract: Hyperspectral data are an important source for monitoring soil salt content on a large scale. However, in previous studies, barriers such as interference due to the presence of vegetation restricted the precision of mapping soil salt content. This study tested a new method for predicting soil salt content with improved precision by using Chinese hyperspectral data, HuanJing-Hyper Spectral Imager (HJ-HSI), in the coastal area of Rudong County, Eastern China. The vegetation-covered area and coastal bare flat area were distinguished by using the normalized differential vegetation index at the band length of 705 nm ($NDVI_{705}$). The soil salt content of each area was predicted by various algorithms. A Normal Soil Salt Content Response Index (NSSRI) was constructed from continuum-removed reflectance (CR-reflectance) at wavelengths of 908.95 nm and 687.41 nm to predict the soil salt content in the coastal bare flat area ($NDVI_{705} < 0.2$). The soil adjusted salinity index (SAVI) was applied to predict the soil salt content in the vegetation-covered area ($NDVI_{705} \geq 0.2$). The results demonstrate that 1) the new method significantly improves the accuracy of soil salt content mapping ($R^2 = 0.6396$, RMSE = 0.3591), and 2) HJ-HSI data can be used to map soil salt content precisely and are suitable for monitoring soil salt content on a large scale.

Keywords: soil salt content; normalized differential vegetation index (NDVI); hyperspectral data; HuanJing-Hyper Spectral Imager (HJ-HSI); coastal area; eastern China

Citation: Li Jianguo, Pu Lijie, Zhu Ming, Dai Xiaoqing, Xu Yan, Chen Xinjian, Zhang Lifang, Zhang Runsen, 2015. Monitoring soil salt content using HJ-1A hyperspectral data: a case study of coastal areas in Rudong County, eastern China. *Chinese Geographical Science*, 25(2): 213–223. doi: 10.1007/s11769-014-0693-2

1 Introduction

Soil salinization is occurring at an increasingly rapid rate around the world; additionally, changing weather patterns associated with climate change are likely to increase this risk (Wei *et al.*, 2001; Gu *et al.*, 2002). Improving methods for soil salt content monitoring and forecasting is currently an important area of research (Metternicht and Zinck, 2003). Traditional methods, including field surveying using Electromagnetic Conductivity Meters (EM38 and EM31) and sample collection do not currently meet the requirements for soil salt content monitoring on a large scale and in areas characterized by high variation (Slavich and Petterson, 1990; Anderson-Cook *et al.*, 2002; Kinal *et al.*, 2006). Previous studies reported that the precision of soil salt content monitoring and mapping based on hyperspectral data was higher than that on multispectral data (Metternicht and Zinck, 2003; Fernandez-Buces *et al.*, 2006; Ghosh *et al.*, 2012; Mashimbye *et al.*, 2012; Shamsi *et*

Received date: 2013-03-04; accepted date: 2013-07-23
Foundation item: Under the auspices of National Natural Science Foundation of China (No. 41230751, 41101547), Scientific Research Foundation of Graduate School of Nanjing University (No. 2012CL14)
Corresponding author: PU Lijie. E-mail: ljpu@nju.edu.cn

al., 2013). The types and levels of soil salinity could be determined accurately by using hyperspectral data with high spectral resolution, which was a generally accepted monitoring method (Farifteh *et al.*, 2008; Weng *et al.*, 2010; Zhang M M *et al*., 2011; Zhang T *et al*., 2011; Ghosh *et al.*, 2012).

Currently, there are problems associated with the use of hyperspectral data to monitor soil salt content. First, though there are many sources of hyperspectral data, satellite-borne sensors are relatively few, and hyperspectral data are most often collected from airborne sensors, including Modular Airborne Imaging Spectrometer (MAIS), Pushroom Hyperspectral Imager (PHI), Operational Modular Imaging Spectrometer (OMIS-1, OMIS-2), Airborne Visible Infrared Imaging Spectrometer (AVIRIS), The Advance of Australian Aerial High Spectral Equipment (HYMAP), and Digital Airborne Imaging Spectrometer (DAIS). Examples of satellite-borne sensors are Moderate-Resolution Imaging Spectroradiometer (MODIS) (Xu *et al*., 2012), Earth Observing 1 (EO-1), and HuanJing-Hyper Spectral Imager (HJ-HSI). Second, although the accuracy of soil salt content monitoring by hyperspectral data is relatively high, most high-salinity soils are located in agricultural or coastal regions where massive crops and halophyte plants on the surface of the land interfere with spectral reflectance (Metternicht and Zinck, 2003). For example, paddy, cotton, and corn crops, as well as halophyte plants, were planted to accelerate salt washing in coastal reclamation areas, which led to a lack of correspondence between the reflectance spectra of soil salt content and the theoretical one measured by the FieldSPec spectrometer, an analytical spectral device (ASD) (Farifteh *et al.*, 2008; Zhang T *et al.*, 2011). Additionally, spectral absorption and reflection vary according to the type of vegetation (Zhang T *et al.*, 2011). Ways to remove the effects of vegetation on the soil reflectance spectra has become an important area of research. Researchers have developed more than ten models to predict soil salt content in many different zones over twenty years, for example, simple ratio vegetation index (RVI), normalized differential vegetation index (NDVI), normalized difference salinity index (NDSI), soil adjusted salinity index (SAVI), partial least squares regression (PLSR), photochemical reflectance index (PRI); plant senescence reflectance index (PERI); and structure-insensitive pigment index (SIPI) (Huete, 1988; Gamon *et al.*, 1997; Blackburn, 1998; Penuelas and Filella, 1998; Merzlyak *et al.*, 1999; Lobell *et al.*, 2010; Weng *et al.*, 2010; Zhang T *et al.*, 2011; Mashimbye *et al.*, 2012). However, the mapping accuracy of previous models is relatively low (Weng *et al.*, 2010; Zhang T *et al.*, 2011; Ghosh *et al.*, 2012). Although some researchers have made great efforts to improve previous models, their accuracy remains low. Reflectance spectra of coastal soils are affected by the presence of vegetation and water (Metternicht and Zinck, 2003), and the contribution of soil salt to the reflectance spectra is hard to distinguish from these interferences (Rao *et al.*, 1995).

Among satellite-borne sensors, MODIS has high time resolution, but also has some inherent shortcomings including low accuracy and low spatial resolution (Lobell *et al.*, 2010; Shamsi *et al.*, 2013). The Hyperion has relatively high spatial resolution (30 m) and high spectral resolution covering a range from visible near infrared (VNIR) to short wave infrared (SWIR); however the width of single image is very narrow, being only 7.7 km. It therefore cannot meet the needs of soil salt content monitoring on a large scale, which restricts its use in practical applications. HJ-HSI is an open access satellite-borne hyperspectral data sensor. It has high spectral resolution (4 nm) and broad coverage: the width of single image is 51 km, and the spatial resolution is 100 m. In this study, we applied HJ-HSI to map the salt content of soils in Rudong County, Jiangsu Province, China. A new method that applies the normal soil salt content response index (NSSRI) and soil adjusted salinity index (SAVI) was applied to map the soil salt content based on $NDVI_{705}$. The objectives of this study are: 1) to confirm the feasibility of using HJ-HSI data to map soil salt content; and 2) to provide a new method of using hyperspectral data for monitoring soil salt content with improved accuracy.

2 Materials and Methods

2.1 Study area

This study was conducted in Rudong County, Jiangsu Province, located in the east coast of China (32°14′23″–32°38′10″N, 120°41′22″–121°35′25″E) (Fig. 1). The study area is close to the Yellow Sea, and has a north subtropical oceanic monsoon climate with plenty of rainfall and sunshine. The average annual temperature is 15℃. The total population in 2010 was 9.96×10^5. The

length of its coast is 106 km, and the coastal area has vast offshore sandbanks. The area of the beach in the study region is vast and shaped by alluvial deposits from the Changjiang (Yangtze) River. The coastal beach is currently expanding seaward at a rate of 25–30 cm a year. At present, 15 reclamation regions have been built up in the study area, and the total area of the reclamation region is 230 km^2 (Fig. 1, Table 1). The area of land that can be reclaimed at present is nearly 100 km^2. The soil is well-developed, and is mostly shallow tidal saline soil. Silty saline soil is the main soil type in the reclamation area, where vegetation coverage is high because of the presence of various crops. In the bare, coastal flat area, sandy saline soil and saline clay are the main soil types. *Suaeda glauca*, *Spartina cynosuroides*, *Spartina alterniflora* and *Spartina patens* are the main vegetation types, but overall vegetation coverage is low. Alluvial soil develops in the flood bed area where there are plenty of freshwater resources. Halophyte plants usually grow in the high tide area.

2.2 Data and processing

2.2.1 Soil Sampling and chemical analyses

This study was conducted from 15 to 19 August, 2011. Four sea-land gradient zones were set up, and one sample was collected every 200 m. The sampling depth was 20 cm, and 64 samples were collected: 26 from the bare flat area and 38 from the vegetation-covered area. Global Positioning System (GPS) was applied to obtain the coordinates of each sampling location. All soil samples were air dried and passed through a 2-mm sieve to remove gravel and weed roots, and then the salt ions and total dissolved salt of each sample were measured. Na^+ and K^+ were measured by flame photometry; CO_3^{2-} and HCO_3^- were determined by using standard H_2SO_4 titration; Mg^{2+}, Ca^{2+}, and SO_4^{2-} were measured by ethylenediaminetetraacetic acid disodium salt (EDTA) complexometry, and Cl^- was determined by standard $AgNO_3$ titration (Bao, 2000). All samples were then passed through a 0.149-mm sieve to determine soil total phosphorus (TP), total nitrogen (TN), total potassium (TK) and soil organic matter (SOM) according to the method of Bao (2000).

2.2.2 Hyperspectral data

The HJ-HSI sensor was carried by the HJ-1A satellite, which was launched on 6 September, 2009. The sensor was activated on 30 September 2009. The HJ-HSI sensor has since provided the first open-access hyperspec-

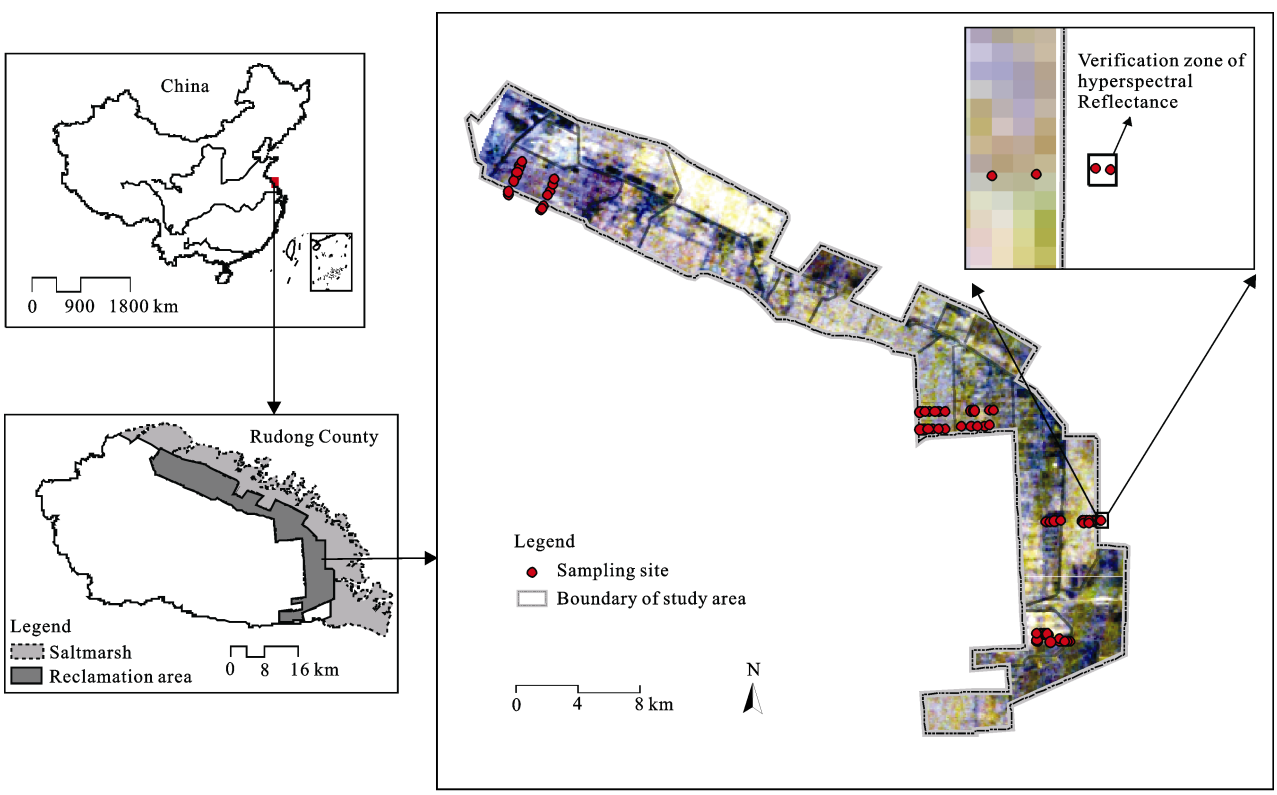

Fig. 1 Map of study area and distribution of sampling sites

Table 1 Reclamation areas in Rudong′s coastal area

Number	Reclamation area	Area (km^2)	Development year
1	Yudong	21.89	2007
2	Yangdong	20.60	1960
3	Wangjiatan	10.14	1974
4	Seconde stage of Yangkou	4.64	2010
5	Seconde stage of Yangbei	1.74	2004
6	First stage of Yangkou	5.03	2004
7	First stage of Yangbei	8.31	2001
8	Rudong saltern	11.87	1958
9	Old Beikan	14.78	1951
10	New Beikan	18.56	1974
11	Juedong	14.29	1972
12	Huangang	13.45	1971
13	Huandong	26.14	1969
14	Dongling	38.64	1982
15	Outside of Huangang	19.77	2007

tral data for environmental monitoring in China. Its spatial resolution is 100 m and it covers a spectral range from 459 nm to 956 nm with a total of 115 bands. The average spectral resolution is 4 nm and the width of a single image is 51 km. The revisit period of the HJ-HSI sensor is four days (Wang *et al.*, 2010). The HJ-HSI data in this study were obtained from the Satellite Environment Center, Ministry of Environmental Protection, China (http://www.secmep.cn/secPortal/portal/index.faces), 450/76 (path/row). The HJ-HSI data loaded from the Satellite Environment Center have been all treated by sensor calibration and radiance calibration. The HJ-HSI data involved in the analysis were acquired on 11 August, 2011. The effect of atmospheric scattering and moisture absorption on reflectance spectra were removed from the image by using the model Line of Sight Atmospheric Analysis of Spectral Hypercubes (FLAASH) in ENVI 4.7 software. The continuum-removed reflectance (CR-reflectance) spectra were acquired by using the continuum removal tools in ENVI 4.7 software to eliminate interference factors, to signal spectral absorption and reflectance to highlight the useful information, and to carry out the experiment on mapping soil salt content.

2.3 Methods

2.3.1 Estimation approach of soil salt content

Crops and halophyte plants are the major barriers to accurately predict the soil salt content (Zhang T *et al.*, 2011). Previous studies have shown a high precision in mapping the soil salt content by using the normalized difference algorithm in the bare flat area (Weng *et al.*, 2010). In the vegetation-covered area, there was a strong correlation between SAVI and soil salt content, while correlations between soil salt content and NDVI, red edge position (REP), plant senescence reflectance index (PSRI), simple ratio (SR), and structure-insensitive pigment index (SIPI) were low (Gitelson and Merzlyak, 1994; Blackburn, 1998; Merzlyak *et al.*, 1999; Aldakheel, 2011). The accuracy of the predicted soil salt content in the vegetation-covered area was lower than that in the coastal bare flat area in those studies, which seriously decreased the accuracy in the whole region. These findings indicate that it is important to distinguish the vegetation-covered area and the bare flat area, and construct corresponding indices accordingly (Fig. 2). Thereby, this study poses a combined indices composed of SAVI and NSSRI to predict soil salt content in the coastal area. In the coastal bare flat area, soil salt content is predicted by using NSSRI. However, soil salt content is estimated by using SAVI in the vegetation-covered area.

This study distinguished the bare flat area and the vegetation-covered area by using $NDVI_{705}$, which is an improved version of NDVI. It is very sensitive to minor changes in the vegetation canopy, gap fraction, and senescence, and has been used in such applications as precision agriculture, forest monitoring, and vegetation stress detection. In addition, it was successfully used as an index to predict the soil salt content by Gitelson and Merzlyak (1994). The formula is as follows:

$$NDVI_{705} = \frac{\rho_{750} - \rho_{750}}{\rho_{750} + \rho_{750}} \tag{1}$$

where ρ_{750} and ρ_{705} are the CR reflectance at 750 nm and 705 nm, respectively. If $NDVI_{705}$ is less than 0.2, the region is considered to be coastal bare flat area; otherwise it is considered as vegetation-covered area.

The normalized difference algorithm was used in the mapping soil salt content to construct the NSSRI in the coastal bare flat area. Its formula is as follows:

$$NSSRI = (B1 - B2) / (B1 + B2) \tag{2}$$

where NSSRI is the normal soil salt content response index; $B1$ and $B2$ are the CR-reflectance of the bands 1 and 2, produced by hyperspectral analysis, respectively.

SAVI was used to predict the soil salt content in the vegetation-covered area. Zhang T *et al.* (2011) revealed

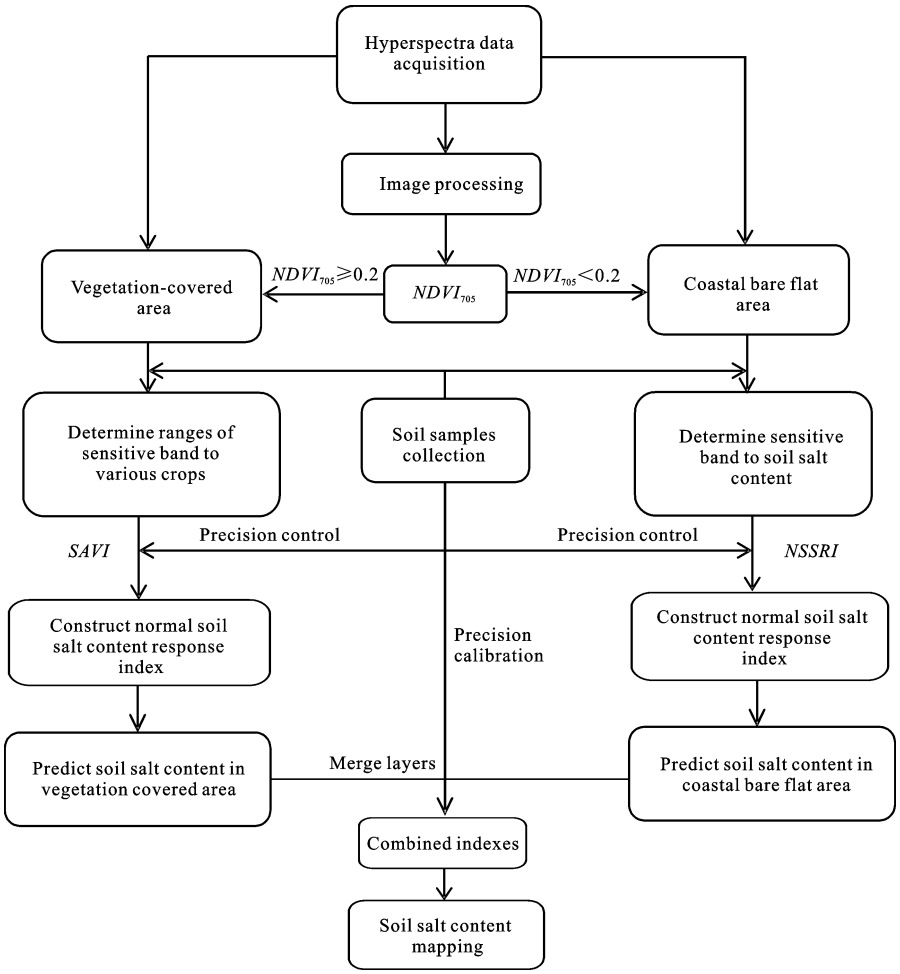

Fig. 2 Description of soil salt content estimation method. $NDVI_{705}$: normalized differential vegetation index; SAVI: soil adjusted salinity index; NSSRI: normal soil salt content response index

differences in the CR-reflectance spectra between different types of vegetation, and a single band could not reflect the impact of all vegetation on the CR-reflectance spectra. Therefore, the soil salt content response index should be constructed with several bands to eliminate the effect of vegetation. Multiple bands can therefore be applied to construct SAVI. Most of the crops and halophyte plants had distinctive CR-reflectance spectra in spectral ranges between 655 nm and 764 nm, and between 889 nm and 903 nm (Zhang T *et al.*, 2011). The average CR-reflectance in the ranges of 655–764 nm and 889–903 nm were therefore applied to construct the SAVI.

$$SAVI = (1+0.5) \times \frac{\lambda_2 - \lambda_1}{\lambda_2 + \lambda_1 + 0.5} \tag{3}$$

where λ_1 and λ_2 are the average CR-reflectance in the ranges of 655–764 nm and 889–903 nm, respectively.

2.3.2 Evaluation of accuracy

The accuracy of mapping was measured by the root mean square error (RMSE) method (Weng *et al.*, 2010).

$$RMSE = \sqrt{\sum_{i=1}^{n} \frac{(y_i - p_i)^2}{n}} \tag{4}$$

where y_i and p_i are the measured soil salt content and predicted soil salt content at the ith sample, respectively, and n is the number of samples involved in the analysis.

3 Results and Analyses

3.1 Descriptive statistics of soil properties in study area

Spectral absorption and reflectance of soils vary depending on the salts present (Farifteh *et al.*, 2008). Ascertaining the type of salts present was therefore an im-

portant step. Descriptive statistics of the soil salt content of the 64 samples was conducted by using SPSS 17.0 software (Table 2 and Table 3). The results show that the predominant ion in the soil in the study area is Cl^-, which is significantly correlated ($p < 0.05$) with total soil salt content, K^+ and Na^+, with correlation coefficients of 0.997, 0.931, and 0.920, respectively. These results indicate that NaCl and KCl are the dominant salts in the soil in the study area. The nutrient content of the soils are relatively low, especially in the coastal bare flat area.

3.2 Spectrum selection

Previous studies have ascertained the most appropriate bands used to determine soil salt content by using the theoretical reflectance curve obtained from the analytical spectral device in the laboratory (Farifteh *et al*., 2006; Fernandez-Buces *et al.*, 2006). The reflectance spectra of soil in the field were disturbed by soil nutrients, physical properties, and moisture, and were therefore not consistent with the corresponding theoretical spectra. The contribution of soil salt was therefore difficult to ascertain (Farifteh *et al.*, 2008; Weng *et al.*, 2010). This study directly assessed and validated the relationship between the CR-reflectance spectra of HJ-HSI and high-salinity soil in the coastal bare flat area. Two samples with high salt content were chosen, and the CR-reflectance spectra were obtained from the five pixels surrounding the two samples (Fig. 1, Table 4). The average CR-reflectance was used to map the soil salt content in the coastal bare flat area (Fig. 3).

The best available pairs of bands must have two features based on the normalized difference algorithm. One is the difference between CR-reflectance of pairs of bands 1 and 2 is very large, another is a high correlation coefficient between the CR-reflectance and the corresponding soil salt content.

The correlation coefficient between the CR-reflectance of different bands and the corresponding soil salt content, as well as the main ions, were calculated to ascertain the best pair of bands (Farifteh *et al.*, 2008) (Fig. 4). The results reveal that high CR-reflectance occurs mainly in

Table 2 Concentrations of ions of soils in study area

Item	CO_3^{2-} (mmol/kg)	HCO_3^- (mmol/kg)	Cl^- (mmol/kg)	SO_4^{2-} (mmol/kg)	K^+ (mmol/kg)	Na^+ (mmol/kg)	Ca^{2+} (mmol/kg)	Mg^{2+} (mmol/kg)	SOM (‰)	TP (‰)	TN (‰)	TK (‰)
Mean	–	4.24	49.38	0.27	0.48	8.73	3.13	11.97	3.44	0.45	0.62	16.23
Minimum	–	3.87	4.12	0.08	0.13	2.83	1.56	5.48	0.17	0.23	0.37	13.97
Maximum	–	4.40	181.44	0.28	1.52	25.92	9.25	22.27	10.54	0.91	0.81	19.29

Table 3 Correlation coefficients among ions and total salt content of soils in study area

	CO_3^{2-}	HCO_3^-	Cl^-	SO_4^{2-}	K^+	Na^+	Ca^{2+}	Mg^{2+}	Total soil salt content
CO_3^{2-}	1	0.054	–0.060	–0.105	–0.073	–0.030	–0.089	0.078	–0.049
HCO_3^-	0.054	1	0.175	0.212*	0.225*	0.235*	0.243*	0.162	0.206
Cl^-	–0.060	0.175	1	0.799**	0.931**	0.920**	0.755**	0.508**	0.997**
SO_4^{2-}	–0.105	0.212*	0.799**	1	0.876**	0.813**	0.610**	0.327**	0.802**
K^+	–0.073	0.225*	0.931**	0.876**	1	0.953**	0.766**	0.430**	0.938**
Na^+	–0.030	0.235*	0.920**	0.813**	0.953**	1	0.747**	0.455**	0.931**
Ca^{2+}	–0.089	0.243*	0.755**	0.610**	0.766**	0.747**	1	0.378**	0.774**
Mg^{2+}	0.078	0.162	0.508**	0.327**	0.430**	0.455**	0.378**	1	0.553**
Total soil salt content	–0.049	0.206	0.997**	0.802**	0.938**	0.931**	0.774**	0.553**	1

Notes: **: significant at the 0.05 level (2-tailed); *: significant at the 0.1 level (2-tailed)

Table 4 Properties of soils in verification zone of CR-reflectance spectra

Sample	Longitude (°)	Latitude (°)	Sampling date	Land use type	pH	a : b : c	Soil salt content (%)
Hb4	121.4	32.33	2011-08-16	Bare shallow	7.97	86 : 4 : 10	0.92
Hb5	121.4	32.33	2011-08-16	Bare shallow	8.06	88 : 2 : 10	0.68

Notes: *a*: the proportion of soil particles greater than 0.05 mm; *b*: the proportion of soil particles between 0.002 mm and 0.05 mm; *c*: the proportion of soil particles less than 0.002 mm

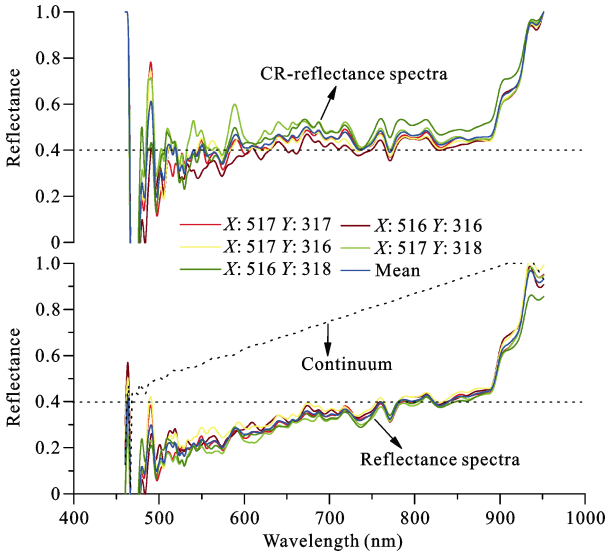

Fig. 3 Continuum-removed reflectance (CR-reflectance) spectra in verification zone (*X*: column; *Y*: row)

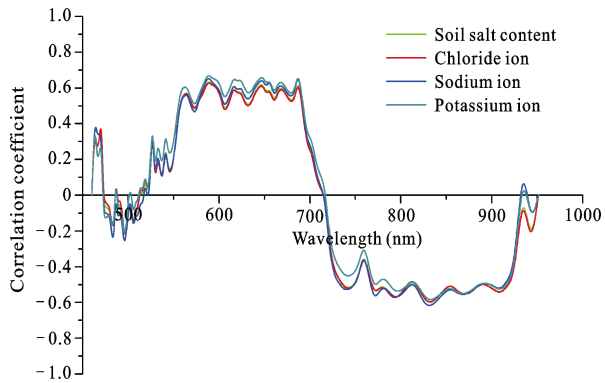

Fig. 4 Correlation coefficient between CR-reflectance and corresponding soil salt content

the ranges of 460–466 nm, 480–494 nm, 587–594 nm, and 900–951 nm, especially in blue bands (460–466 nm) and NIR bands (900–951 nm) (Fig. 3). The correlation coefficient between the CR-reflectance and the corresponding soil salt content is high ($r > 0.5$) in the ranges of 558–688 nm and 778–909 nm (Fig. 4). The highest value is at the wavelength of 687.41 nm ($r = 0.66$). Two available pairs of bands are determined based on the requirements of the normalized difference algorithm (908.95 and 687.41 nm; 908.95 and 834.27 nm). The correlation coefficients are relatively high in the first pair, −0.55 and 0.66, respectively, and the CR-reflectance values are 0.620 and 0.488, respectively. The CR-reflectance values in the second pair are 0.620 and 0.438, respectively, and their correlation coefficients are −0.55 and −0.60, respectively. This indicates that the first pair is more sensitive to the changes in the CR-reflectance that result from changes in the soil salt content than the second pair. So, the index NSSRI was constructed by using the wavelengths of 908.95 nm and 687.41 nm.

$$NSSRI = (ref_{908.95} - ref_{687.41}) / (ref_{908.95} + ref_{687.41}) \quad (5)$$

where $ref_{908.95}$ and $ref_{687.41}$ are the CR-reflectance at the wavelengths of 908.95 nm and 687.41 nm, respectively.

3.3 Accuracy of soil salt content prediction

The coastal bare flat area ($NDVI_{705} < 0.2$) and the vegetation covered area ($NDVI_{705} \geq 0.2$) were extracted by ENVI 4.7 software (Verrelst *et al.*, 2008). Equation (5) was applied to calculate the NSSRI in the coastal bare flat area, and SAVI (Equation (3)) was applied in the vegetation-covered area. Linear regression fitting analysis between measured soil salt content and NSSRI, SAVI was conducted by using Excel software. Eighteen of the 26 samples located in the coastal bare flat area were used to conduct the model for estimating soil salt content by using NSSRI (Fig. 5). Thirty of the 38 samples located in the vegetation-covered area were used to construct the model for estimating the soil salt content by using SAVI (Fig. 6). The other 16 samples (eight in the coastal bare flat area and eight in the vegetation covered area) were used to test the combined indices model as posed above (Fig. 7, Table 5).

Figures 5 and 6 show that the fitting accuracy of the soil salt content predicted with NSSRI and SAVI was relatively higher than that from the results of Zhang T *et al.* (2011) (R^2 between 0.50 and 0.58), especially in the coastal bare flat area (R^2 = 0.8227, RMSE = 0.1440), which was in agreement with Gamon *et al.* (1997), Merzlyak *et al.* (1999) and Weng *et al.* (2010).

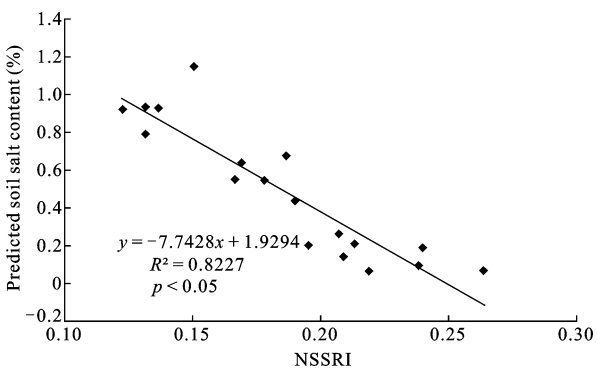

Fig. 5 Linear regression function of soil salt content based on normal soil salt content response index (NSSRI) in coastal bare flat area

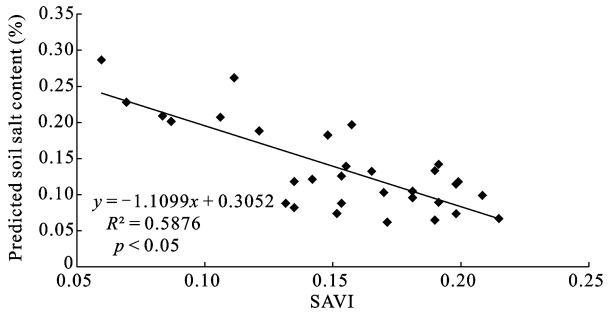

Fig. 6 Linear regression function of soil salt content based on soil adjusted salinity index (SAVI) in vegetation-covered area

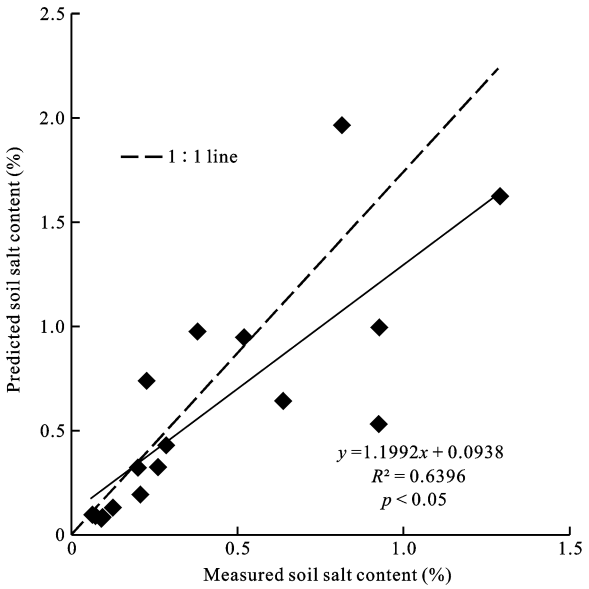

Fig. 7 Comparison of predicted and measured soil salt content in 2011 in study area

Table 5 Comparison of accuracy of soil salt content estimation based on different methods

Study	R^2	RMSE
Gitelson and Merzlyak (1994)	0.4335	0.7291
Merzlyak *et al*. (1999)	0.3212	0.3652
This study	0.6396	0.3591

As mentioned above, a scatter plot of the predicted soil salt content and its corresponding measured values was obtained by using 16 samples (Fig. 7). As shown in Table 5, accuracy comparison between this study and other two results was conducted. The model used by Gitelson and Merzlyak (1994) was based on an index of SR_{705}, which is the ratio of CR-reflectance in 750 nm to that in 705 nm ($SR_{705} = R_{750} / R_{705}$). And that ulitilized by Merzlyak *et al*. (1999) was based on the index of PSRI defined as the ratio of CR-reflectance in 680 nm subtract that in 500 nm to that in 750 nm ($PSRI = (R_{680} - R_{500}) / R_{750}$). From Table 5, we can known that the prediction accuracy of the method proposed in this study was highest (R^2 = 0.6396, RMSE = 0.3591), indicating that this new method is appropriate to use to monitor soil salt content because it has been shown to predict soil salt content with precision.

3.4 Spatial pattern of predicted soil salt content

The map of soil salt content in the study area was obtained by merging maps of the coastal bare flat area and the vegetation-covered area (Fig. 8). As shown in Fig. 8, soil salt content in the study area generally varied from 0 to 3.2%. Soil with a high salt content (> 2%) are mainly located within the newly reclaimed area and its peripheral region (coastal bare flat area). Soils with the highest salt content are located in the Rudong saltern reclamation area and its peripheral bare flat region, the Yangkou reclamation area and the unused marsh in its southeastern part; in some of these areas, the salt content exceeds 3%. This is likely because of the location of these regions are mainly in the lunar submerged tidal zone, comprising beach salty soil where many salterns have carried out solar salt production and the soil salt content in the topsoil is high (Fang *et al.*, 1990). The spatial pattern of soil salt content in the study area is as a gradient, and soils closest to the coast have the highest salt content. This gradient effect is most obvious in the reclamation areas of Yangdong, Huandong, Huangang, Dongling, and their peripheral bare flat regions. The results also demonstrate that soil salt content decreases with increasing time since reclamation.

4 Discussion

With respect to previous studies, the accuracy of the model developed in this study was high when used to predict soil salt content (R^2 = 0.6396, RMSE = 0.3591) (Weng and Gong, 2006; Ghosh *et al.*, 2012). The model performed well, likely because different indices were combined to predict soil salt content of the vegetation-covered area and the coastal bare flat area. Linear models for mapping soil salt content based on hyperspectral data all produce abnormal values (Gamon *et al.*, 1997; Merzlyak *et al.*, 1999; Weng *et al.*, 2010; Xu *et al.*, 2012; Su *et al*., 2013). The soil salt content of the coastal marsh range from 0.1% to 3% (Fang *et al.*, 1990); however these models in some cases predict

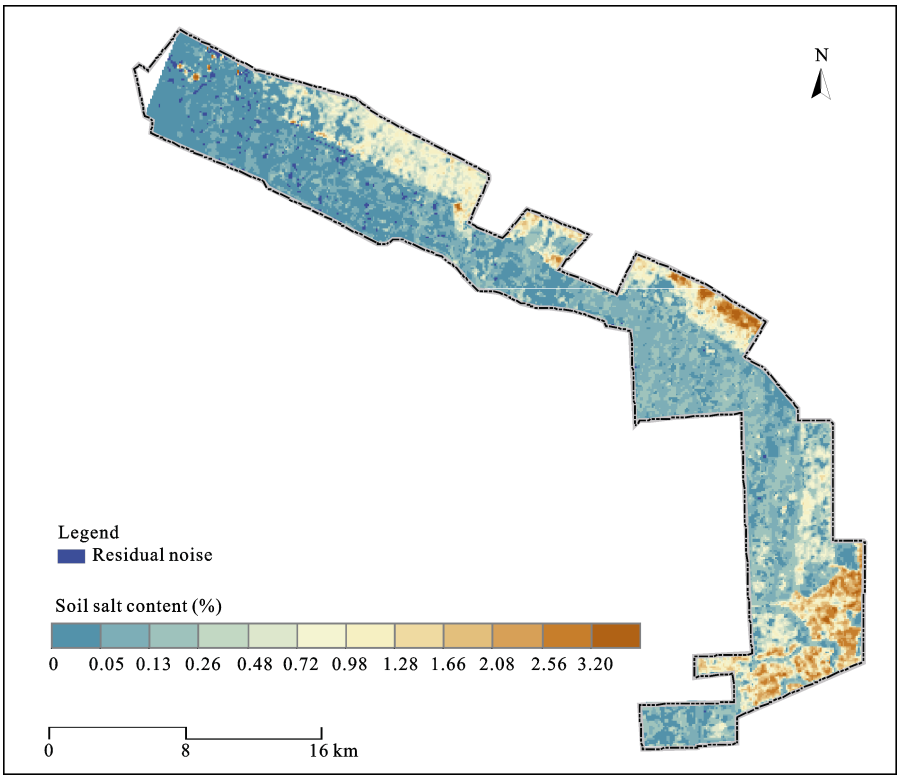

Fig. 8 Map of predicted soil salt content by combined indices model in study area

negative values. For example, in the north of the study area (the north bank of the Nanling River), the predicted soil salt content by using the method proposed by this study is −11% and −6%. The pixels with negative values were usually affected by residual noise in the image after atmospheric correction by the Fast Line-of-sight Atmospheric Analysis of Spectral Hypercubes (FLAASH) model, such as image noise or clouds (Weng *et al.*, 2010). In the Nanling River Estuary, the soil salt content values predicted by the method ranged from −0.400% to −0.001%. The main reason for this inaccuracy is likely the presence of non-saline soils, which result from the use of freshwater from the Nanling River for washing and irrigation; these activities cause a decrease in the topsoil salt content in the Nanling River Estuary and its surrounding area. Negative values were assigned a value of 0 in this study. The values of soil salt content are very high in some pixels, and some of them are greater than 7%. The areas with high values are mainly located in the coastal bare flat areas where there are many salterns, fish ponds, and wide water bodies, which can lead to abnormal changes in the soil salt content response indices (NSSRI and SAVI).

Currently, the most popular models for constructing soil salt content response indices are ratio algorithm (Merzlyak *et al.*, 1999), difference algorithm (Huete, 1988), differential trend algorithm (Horler *et al.*, 1983), and normalized difference algorithm (Gitelson and Merzlyak, 1994; Gamon *et al.*, 1997). Commonly, the soil salt content response index is constructed by using a single algorithm based on the best bands that were sensitive to soil salt content, which enhances the signal from soil salt and eliminates background noise of the soil due to vegetation, water, or soil nutrients. However, the reflectance spectra of one or two bands can not accurately represent the soil salt content because of interference due to moisture and vegetation. Currently, the major models for mapping soil salt content are those constructed by only one or two bands, or four bands at the most. This is another reason for the low accuracy of soil salt content maps. New models should be constructed involving more bands more sensitive to the presence of soil ions by using multiple regression analysis to improve the precision of soil salt content predictions. Furthermore, quantitative relationships may be built between reflectance and various salt ions directly. If this could be done, then researchers would be able to quickly determine the soil salt content based on hyperspectral data; however this would require extensive laboratory work.

Previous studies have reported the mapping of soil salt content by using hyperspectral data in arid and semi-arid areas in general have high accuracy with R^2 between 0.7–0.9 (Dutkiewicz *et al.*, 2009; Bilgili *et al.*, 2011; Ding *et al.*, 2011; Mashimbye *et al.*, 2012). In the coastal areas, mapping accuracy tends to be relatively low because of the high moisture content of soils. The reflectance spectra of various types and levels of salt in air-dried or oven-dried soils have been accurately obtained (Metternicht and Zinck, 2003; Farifteh *et al.*, 2008); however the difference between reflectance spectra of land covered by crops and land covered by halophyte plants were small, which indicates the need for more fieldwork (Zhang T *et al.*, 2011). Active remote sensing technology may be an effective way to resolve the problem of mapping soil salinity (Metternicht and Zinck, 2003; Ding and Yao, 2013). Previous studies have found that soil organic matter, texture, and metal, moisture and nutrient content all influenced reflectance spectra (Gallagher *et al.*, 2008; Mulder *et al.*, 2011). Methods to identify the combined effects of various factors on reflectance of soil should be a focus of future research.

5 Conclusions

Hyperspectral data are currently an important source for mapping soil salt content. However, vegetation, soil moisture, and soil texture are the barriers restricting the precision of soil salt content mapping in the coastal areas. Combined indices or integrated models involving multiple factors may be effective ways to improve the accuracy of soil salt content maps. In this study, a new methods with multiple indices were successfully used to predict soil salt content in Rudong County, Jiangsu Province, China. In the study area, the main salts in the coastal reclamation area are NaCl and KCl. This study attempted to restrict the interference by vegetation using $NDVI_{705}$ and applied different indices to map soil salt content in the coastal bare flat area and vegetation-covered area. Soil salt content is significantly correlated with CR-reflectance at the band length of 908.95 nm and 687.41 nm, with correlation coefficient of −0.55 and 0.66, respectively. NSSRI and SAVI are applied to indirectly explain the soil salt content in the coastal bare flat area and vegetation-covered area respectively. The results show that the accuracy of the new method (R^2 = 0.6396, RMSE = 0.3591) is higher than that of previous studies that use a single index. This study indicates that HJ-HSI data have enormous potential to predict the soil salt content on a large scale.

Acknowledgements

Special thanks go to Professor DU Peijun of the Department of Geographic Information Science, Nanjing University, China for his helpful suggestions; we also thank Doctoral candidate LYV Chunguang of International Institute for Earth System Science, Nanjing University for his help in hyperspectral data preprocessing.

References

Aldakheel Y Y, 2011. Assessing NDVI spatial pattern as related to irrigation and soil salinity management in Al-Hassa Oasis, Saudi Arabia. *Journal of the Indian Society of Remote Sensing*, 39(2): 171–180. doi: 10.1007/s12524-010-0057-z

Anderson-Cook C M, Alley M, Roygard J *et al.*, 2002. Differentiating soil types using electromagnetic conductivity and crop yield maps. *Soil Science Society of America Journal*, 66(5): 1562–1570. doi: 10.2136/sssaj2002.1562

Bao Shidan, 2000. *Soil and Agricultural Chemistry Analysis*. Beijing: Agriculture Publication, 355–356. (in Chinese)

Bilgili A V, Cullu M A, van Es H *et al.*, 2011. The use of hyperspectral visible and near infrared reflectance spectroscopy for the characterization of salt-affected soils in the Harran Plain, Turkey. *Arid Land Research and Management*, 25(1): 19–37. doi: 10.1080/15324982.2010.528153

Blackburn G A, 1998. Quantifying chlorophylls and caroteniods at leaf and canopy scales: An evaluation of some hyperspectral approaches. *Remote Sensing of Environment*, 66(3): 273–285.

Ding J L, Wu M C, Tiyip T, 2011. Study on soil salinization information in arid region using remote sensing technique. *Agricultural Sciences in China*, 10(3): 404–411. doi: 10.1016/S1671-2927(11)60019-9

Ding Jianli, Yao Yuan, 2013. Evaluation of soil moisture contents under sparse vegetation coverage conditions using microwave remote sensing technology in arid region. *Scientia Geographica Sinica*, 33(7): 837–843. (in Chinese)

Dutkiewicz A, Lewis M, Ostendorf B, 2009. Evaluation and comparison of hyperspectral imagery for mapping surface symptoms of dryland salinity. *International Journal of Remote Sensing*, 30(3): 693–719. doi: 10.1080/01431160802392612

Farifteh J, Farshad A, George R, 2006. Assessing salt-affected soils using remote sensing, solute modelling, and geophysics. *Geoderma*, 130(3): 191–206. doi: 10.1016/j.geoderma.2005.02.003

Farifteh J, van der Meer F, van der Meijde M *et al.*, 2008. Spectral characteristics of salt-affected soils: A laboratory experiment. *Geoderma*, 145(3–4): 196–206. doi: 10.1016/j.geoderma.2008.03.011

Fang Ming, Chen Bangben, Hu Rongqin *et al.*, 1990. Ecological

salinization characters of sea beach soil in Jiangsu. *Acta Pedologica Sinica*, 27(3): 335–342. (in Chinese)

Fernandez-Buces N, Siebe C, Cram S *et al*., 2006. Mapping soil salinity using a combined spectral response index for bare soil and vegetation: A case study in the former lake Texcoco, Mexico. *Journal of Arid Environments*, 65(4): 644–667. doi: 10.1016/j.jaridenv.2005.08.005

Gallagher F J, Pechmann I, Bogden J D *et al*., 2008. Soil metal concentrations and productivity of Betula populifolia (gray birch) as measured by field spectrometry and incremental annual growth in an abandoned urban Brownfield in New Jersey. *Environmental Pollution*, 156(3): 699–706. doi: 10.1016/j.envpol.2008.06.013

Gamon J, Serrano L, Surfus J, 1997. The photochemical reflectance index: An optical indicator of photosynthetic radiation use efficiency across species, functional types, and nutrient levels. *Oecologia*, 112(4): 492–501. doi: 10.1007/s004420050337

Ghosh G, Kumar S, Saha S, 2012. Hyperspectral satellite data in mapping salt-affected soils using linear spectral unmixing analysis. *Journal of the Indian Society of Remote Sensing*, 40(1): 129–136. doi: 10.1007/s12524-011-0143-x

Gitelson A, Merzlyak M N, 1994. Spectral reflectance changes associated with autumn senescence of aesculus hippocastanum L. and Acer platanoides L. leaves. spectral features and relation to chlorophyll estimation. *Journal of Plant Physiology*, 143(3): 286–292. doi:10.1016/S0176-1617(11)81633-0

Gu Fengxue, Zhang Yuandong, Chu Yu *et al*., 2002. Primary analysis on groundwater, soil moisture and salinity in Fukang Oasis of Southern Junggar Basin. *Chinese Geographical Science*, 12(4): 333–338. doi:10.1007/s11769-002-0038-4

Horler D, Dockray M, Barber J, 1983. The red edge of plant leaf reflectance. *International Journal of Remote Sensing*, 4(2): 273–288. doi: 10.1080/01431168308948546

Huete A R, 1988. A soil-adjusted vegetation index (SAVI). *Remote Sensing of Environment*, 25(3): 295–309. doi: 10.1016/0034-4257(88)90106-X

Kinal J, Stoneman G, Williams M, 2006. Calibrating and using an EM31 electromagnetic induction meter to estimate and map soil salinity in the jarrah and karri forests of south-western Australia. *Forest Ecology And Management*, 233(1): 78–84. doi: 10.1016/j.foreco.2006.06.003

Lobell D, Lesch S, Corwin D *et al*., 2010. Regional-scale assessment of soil salinity in the Red River Valley using multi-year MODIS EVI and NDVI. *Journal of Environmental Quality*, 39(1): 35–41. doi: 10.2134/jeq2009.0140

Mashimbye Z E, Cho M A, Nell J P *et al*., 2012. Model-based integrated methods for quantitative estimation of soil salinity from hyperspectral remote sensing data: A case study of selected south African soils. *Pedosphere*, 22(5): 640–649. doi: 10.1016/S1002-0160(12)60049-6

Merzlyak M N, Gitelson A A, Chivkunova O B *et al*., 1999. Non-destructive optical detection of pigment changes during leaf senescence and fruit ripening. *Physiologia Plantarum*, 106(1): 135–141. doi: 10.1034/j.1399-3054.1999.106119.x

Metternicht G, Zinck J, 2003. Remote sensing of soil salinity: Potentials and constraints. *Remote Sensing of Environment*, 85(1): 1–20. doi: 10.1016/S0034-4257(02)00188-8

Mulder V L, de Bruin S, Schaepman M E *et al*., 2011. The use of remote sensing in soil and terrain mapping—A review. *Geoderma*, 162(1-2): 1–19. doi: 10.1016/j.geoderma.2010.12.018

Penuelas J, Filella I, 1998. Visible and near-infrared reflectance techniques for diagnosing plant physiological status. *Trends In Plant Science*, 3(4): 151–156. doi: 10.1016/S1360-1385(98)01213-8

Rao B R M, Sankar T R, Dwivedi R S *et al*., 1995. Spectral behavior of salt-affected soils. *International Journal of Remote Sensing*, 16(12): 2125–2136. doi: 10.1080/01431169508954546

Shamsi S R F, Zare SAbtahi S A, 2013. Soil salinity characteristics using moderate resolution imaging spectroradiometer (MODIS) images and statistical analysis. *Archives of Agronomy and Soil Science*, 59(4): 471–489. doi: 10.1080/03650340.2011.646996

Slavich P, Petterson G, 1990. Estimating average rootzone salinity from electromagnetic induction (EM-38) measurements. *Soil Research*, 28(3): 453–463. doi: 10.1071/SR9900453

Su Zilong, Zhang Guanghui, Yu Yan, 2013. Soil moisture characteristic of different land use types in the typical black soil region of northeast China. *Scientia Geographica Sinica*, 33(9): 1104–1110. (in Chinese)

Verrelst J, Schaepman M E, Koetz B *et al*., 2008. Angular sensitivity analysis of vegetation indices derived from CHRIS/PROBA data. *Remote Sensing of Environment*, 112(5): 2341–2353. doi: 10.1016/j.rse.2007.11.001

Wang Qiao, Wu Chuanqing, Li Qing *et al*., 2010. Chinese HJ-1A/B satellites and data characteristics. *Science China* (*Earth Sciences*), 53(1): 51–57. doi: 10.1007/s11430-010-4139-0

Wei D, Yan H, Song X S *et al*., 2001. Hydrochemical characteristics of salt marsh wetlands in western Songnen Plain. *Journal of Geographical Sciences*, 11(2): 217–223. doi: 10.1007/BF02888693

Weng Y, Gong P, Zhu Z, 2010. A spectral index for estimating soil salinity in the Yellow River Delta region of China using EO-1 Hyperion data. *Pedosphere*, 20(3): 378–388. doi: 10.1016/S1002-0160(10)60027-6

Weng Yongling, Gong Peng, 2006. A review on remote sensing technique for salt affected soils. *Scientia Geographica Sinica*, 26(3): 369–375. (in Chinese)

Xu Yongming, Zhao Qiaohua, Ba Yaer *et al*., 2012. Spatio- temporal variations of land surface evapotranspiration of Bosten Lake Basin based on MODIS data. *Scientia Geographica Sinica*, 32(11): 1353–1357. (in Chinese)

Zhang M M, SuY P, Wu P, 2011. Using HJ-I satellite remote sensing data to surveying the Saline soil distribution in Yinchuan Plain of China. *African Journal of Agricultural Research*, 6(32): 6592–6597. doi: 10.5897/AJAR11.130

Zhang T, Zeng S, Gao Y *et al*., 2011. Using hyperspectral vegetation indices as a proxy to monitor soil salinity. *Ecological Indicators*, 11(6): 1552–1562. doi: 10.1016/j.ecolind.2011.03.025